Int. J. Solids Structures Vol. 30, No. 5, pp. 659–673, 1993
Printed in Great Britain

0020–7683/93 $6.00+ .00

QUASI-STATIC CRACK GROWTH IN MATERIALS DISPLAYING THE BAUSCHINGER EFFECT—I. STEADY-STATE ANALYSIS

R. NARASIMHAN
Department of Mechanical Engineering, IISc, Bangalore 560012, India

C. S. VENKATESHA
Government College of Engineering, Davangere 577004, India

and

S. SAIRAM
Brown University, Providence, RI 02912, U.S.A.

(*Received* 21 *October* 1991; *in revised form* 20 *July* 1992)

Abstract—In this paper, steady-state quasi-static crack growth in an elastic–plastic material is analysed under Mode III and Mode I plane stress small-scale yielding conditions using a finite element procedure. The material is assumed to obey an incremental plasticity theory with linear isotropic or kinematic hardening. The influence of the Bauschinger effect on the stress distribution near the crack tip and crack opening profiles is examined. The results show that for Mode III and Mode I plane stress, the near-tip angular stress variation for kinematic hardening dos not deviate significantly from that for isotropic hardening except in the region behind the crack tip. A ductile fracture criterion is used to estimate the ratio J_{ss}/J_c of the far-field J integral for steady-state crack growth to that crack initiation. This ratio is substantially smaller for kinematic hardening (as compared to isotropic hardening) which implies that the Bauschinger effect will diminish the capacity of an elastic–plastic material to sustain stable crack growth under Mode III and Mode I plane stress.

1. INTRODUCTION

In elastic–plastic materials, a slow, stable crack extension phase is often observed prior to catastrophic failure, during which a steady increase in applied load or displacement condition is required. The main source for stable crack growth is the increased resistance displayed by an elastic–plastic material to strong non-proportional loading that is experienced in the vicinity of the propagating crack tip. This results in lessened strain concentration at the extending crack tip as compared to a stationary crack tip which is subjected to monotonic loading. It must be emphasized that the above phenomenon is primarily caused by crack-tip plasticity.

Quasi-static crack growth in elastic–plastic materials has been analysed by several investigators. Chitaley and McClintock (1971) found an asymptotic solution for a crack growing quasi-statically in an elastic–perfectly plastic material under Mode III. Drugan *et al.* (1982) assembled an asymptotic field for cracks growing in an elastic–perfectly plastic material under Mode I plane strain conditions. Amazigo and Hutchinson (1977) obtained asymptotic steady-state solutions for Mode I (plane strain and plane stress) and Mode III crack propagation in isotropic linear hardening solids. Their analysis neglected the possible occurrence of secondary plastic reloading near the crack flank. This was taken into account by Castañeda (1987). His results indicate that the effect of plastic reloading on the singularity order of the crack tip fields is significant only for Mode I plane strain. The above issue was also considered in the work of Zhang *et al.* (1983) who studied Mode I plane strain crack growth in materials displaying a combination of (linear) isotropic and kinematic hardening.

Finite element simulations of both steady-state and transient (stable) quasi-static crack growth have been performed by many researchers. The main objectives of these studies have been to examine the validity of the analytical asymptotic solutions and to investigate the general nature of the material resistance curves. Sham (1983) and Narasimhan *et al.* (1987a, b) carried out detailed finite element analyses of stable crack growth under Mode I

plane strain and plane stress conditions, respectively. In these studies, a nodal release procedure was used to simulate slow, stable crack extension. Sham (1983) considered only elastic–perfectly plastic materials, whereas Narasimhan *et al.* (1987a, b) analysed crack growth in both non-hardening and isotropic power law hardening materials. An important observation made by Narasimhan *et al.* (1987b) was that stable crack growth under Mode I plane stress could be far more extensive than in Mode I plane strain.

Dean and Hutchinson (1980) and Lam and McMeeking (1984) have used a finite element formulation based on moving crack tip coordinates to simulate steady-state quasi-static crack growth under Mode III and Mode I plane strain conditions. Dean (1983) has used the methodology of Dean and Hutchinson (1980) to analyse Mode I plane stress crack growth in linear isotropic hardening solids. The above investigations have demonstrated that, in general, the potential of an elastic–plastic material for stable crack growth will be greatly diminished in the presence of isotropic strain hardening.

It should be noted that anisotropic hardening such as corner formation on the yield surface and the Bauschinger effect needs to be considered in crack growth analyses because of the strong non-proportional loading history experienced by a material point when the crack tip passes underneath (or above) it. Dean and Hutchinson (1980) studied the influence of corner formation on the yield surface on Mode III crack growth. For Mode I plane strain crack growth, Lam and McMeeking (1984) made a comprehensive assessment of the influence of both corner formation as well as the Bauschinger effect. Although the results of Dean and Hutchinson (1980) for Mode III are not sufficiently conclusive, Lam and McMeeking (1984) found that anisotropic hardening further decreased the capacity of a material to sustain stable crack growth under Mode I plane strain. Thus, in this sense, analysis of slow crack growth based on a smooth yield surface with isotropic strain hardening may provide unconservative estimates regarding the potential of the material for stable crack extension.

The influence of anisotropic hardening on Mode I plane stress crack growth has not been examined. It is important to investigate this issue in detail because of the following reasons. Firstly, as noted earlier, analysis using isotropic hardening conducted by Narasimhan *et al.* (1987b) has shown that stable crack growth under Mode I plane stress could be far more extensive than in Mode I plane strain. Thus, it would be of interest to examine whether anisotropic hardening considerably reduces this vast potential for stable crack growth under plane stress. Secondly, the mechanics of deformation near a growing crack tip in an elastic–plastic material under Mode I plane stress is known to be quite different from Mode I plane strain [see, for example, Rice (1975)]. Hence, the conclusions of Lam and McMeeking (1984) regarding the effect of anisotropic hardening on Mode I plane strain crack extension are not directly relevant to the plane stress case. Finally, plane stress crack growth has tremendous practical importance, as for example, to thin aircraft structures.

It is the objective of this work to analyse Mode I plane stress quasi-static crack growth in materials displaying the Bauschinger effect and to make quantitative comparisons with isotropically hardening materials regarding the near-tip fields and the resistance to crack growth. For this purpose, materials that exhibit both linear isotropic and linear kinematic hardening are considered. In Part I of the work, which is presented in this paper, steady-state crack growth under small-scale yielding conditions is simulated. An investigation of transient (stable) crack growth is taken up in Part II. In order to clearly understand some of the underlying issues, the simpler Mode III case is first considered. It is well known from analytical studies [see, for example, Rice (1975)] that certain features in the asymptotic fields for Mode I plane stress crack growth are qualitatively similar to Mode III.

The organization of this paper is as follows. In Section 2, the constitutive models that are used are presented. In Section 3, the finite element procedure employed to simulate steady-state crack growth is briefly described. In Section 4, the results obtained from the analyses are discussed. The finite element meshes used in this work are well refined near the crack tip so that an accurate modelling of the near-tip fields is achieved. This is confirmed by a good comparison between the present numerical results and the analytical (asymptotic) solutions of Castañeda (1987) for linear isotropic hardening (see Section 4).

The influence of the Bauschinger effect on the stress distribution near the crack tip and the crack opening profile is examined for Mode III and Mode I plane stress. By using a critical crack opening displacement criterion for both crack initiation and continued crack growth, the ratio J_{ss}/J_c, of the far-field J integral for steady-state crack growth to that at initiation, is estimated. This ratio is expected to provide an indication of the potential of the material for stable crack growth. A comparison of this ratio for linear isotropic and kinematic hardening is made with the view of assessing the influence of the Bauschinger effect on the material resistance to quasi-static crack growth.

2. CONSTITUTIVE MODEL

In this paper, a small strain, incremental plasticity theory is employed along with the Huber–von Mises yield condition and the associated flow rule. The material is assumed to display a *bilinear* response to uniaxial tension. Materials that exhibit pure isotropic or pure kinematic hardening under plastic deformation are considered. The latter has been proposed as a simple model to describe the Bauschinger effect (i.e. reduced yield stress following reversed uniaxial loading) which is observed in many engineering materials. A general description of the material model (which incorporates combined isotropic-kinematic hardening) is presented below. Specialization of the constitutive equations to anti-plane shear is straightforward and is not given here.

The Huber–von Mises yield condition for combined isotropic-kinematic hardening can be expressed as:

$$\Phi(\sigma_{ij}, \sigma_y, \alpha_{ij}) = \tfrac{3}{2}(S_{ij}-\alpha_{ij})(S_{ij}-\alpha_{ij})-\sigma_y^2 = 0. \tag{1}$$

Here, S_{ij} is the deviatoric stress tensor and α_{ij} is the *back stress* tensor that describes the translation of the center of the yield surface in deviatoric stress space. Also, σ_y is a parameter which is related to the size of the yield surface and is identified with the yield stress under uniaxial tension for pure isotropic hardening. The initial value of σ_y is denoted by σ_0. In the present work, the center of the yield surface for the virgin material is assumed to be at the origin in deviatoric stress space, so that initially $\alpha_{ij} = 0$.

Within the context of the small strain flow theory of plasticity, the total strain rate tensor can be decomposed into elastic and plastic parts as:

$$\dot{\varepsilon}_{ij} = \dot{\varepsilon}^e_{ij}+\dot{\varepsilon}^p_{ij}. \tag{2}$$

The stress rate tensor $\dot{\sigma}_{ij}$ is related to the elastic strain rate tensor $\dot{\varepsilon}^e_{ij}$ through a constant, isotropic, positive definite elasticity tensor C_{ijkl} as,

$$\dot{\sigma}_{ij} = C_{ijkl}\dot{\varepsilon}^e_{kl}. \tag{3}$$

The associated flow rule takes the form,

$$\dot{\varepsilon}^p_{ij} = \dot{\lambda}v_{ij}, \tag{4a}$$

where

$$v_{ij} = \frac{\partial\Phi}{\partial\sigma_{ij}} = 3(S_{ij}-\alpha_{ij}). \tag{4b}$$

In these equations, v_{ij} represents the normal to the yield surface in stress space and $\dot{\lambda} \geqslant 0$ is a plastic parameter.

The description of the material model is completed by specifying appropriate evolution equations for the plastic internal variables σ_y and α_{ij}. The evolution equation for σ_y is given by:

$$\dot{\sigma}_y = \beta H \dot{\varepsilon}^{\mathrm{p}}_{\mathrm{eqv}}. \tag{5}$$

Here, $\dot{\varepsilon}^{\mathrm{p}}_{\mathrm{eqv}} = \sqrt{2/3\dot{\varepsilon}^{\mathrm{p}}_{ij}\dot{\varepsilon}^{\mathrm{p}}_{ij}}$ is the equivalent plastic strain rate and $H = EE_{\mathrm{t}}/(E-E_{\mathrm{t}})$, where E_{t} is the tangent modulus of the material which is obtained from the bilinear uniaxial response.† Also, β is a parameter which is taken as zero for pure kinematic hardening and as unity for pure isotropic hardening.

In this paper, Prager's hardending rule is used to describe the translation of the yield surface. This assumes that the yield surface moves in the direction of the plastic strain increment, so that,

$$\dot{\alpha}_{ij} = (1-\beta) b \dot{\varepsilon}^{\mathrm{p}}_{ij}. \tag{6}$$

In the above equation, b is a positive constant, which can be obtained from the bilinear uniaxial response as $b = 2H/3$.

By using eqns (1)–(6), and plastic consistency, the constitutive law for material currently experiencing plastic deformation can be expressed as,

$$\dot{\sigma}_{ij} = M_{ijkl}\dot{\varepsilon}_{kl} = \left[C_{ijkl} - \frac{C_{ijpq}\nu_{pq}\nu_{mn}C_{mnkl}}{\nu_{rt}C_{rtuv}\nu_{uv} + 4\sigma_y^2 H} \right] \dot{\varepsilon}_{kl}. \tag{7}$$

For plane stress, the equations given above are used along with the constraint conditions $\sigma_{3i} \equiv 0$.

3. NUMERICAL PROCEDURE

In this paper, steady-state crack growth is simulated under Mode III and Mode I plane stress using the finite element procedure based on moving crack tip coordinates devised by Dean and Hutchinson (1980). Herein, a semi-infinite crack propagating in a quasi-static manner under small-scale yielding conditions is considered. It is assumed that the zone of inelastic deformation is contained in a small region near the crack tip and the elastic K-field holds good at points far away from the tip. A brief description of the numerical procedure is given below.

3.1. *Mode III crack growth*

In this case, there are only two stress components $\tau_1 = \sigma_{31}$ and $\tau_2 = \sigma_{32}$, and two strain components $\gamma_1 = 2\varepsilon_{31}$ and $\gamma_2 = 2\varepsilon_{32}$. Also, the only non-zero displacement component is $u_3(x_1, x_2)$. The above quantities and the (moving) crack-tip coordinates (x_1, x_2) are normalized as follows:

$$\left.\begin{aligned} \hat{x}_i &= x_i/(K/\tau_0)^2 \\ \hat{u}_3 &= u_3/(K^2/G\tau_0) \\ \hat{\gamma}_i = \gamma_i/\gamma_0 \quad &\text{and} \quad \hat{\tau}_i = \tau_i/\tau_0 \end{aligned}\right\}. \tag{8}$$

Here, τ_0 is the initial yield stress (in simple shear), $\gamma_0 = \tau_0/G$ is the initial yield strain (in simple shear), G is the shear modulus and K is the remote stress intensity factor. Further, the crack is assumed to propagate steadily in the x_1 direction with velocity v, so that the time rate of change of any field quantity at a fixed material point can be expressed as:

† For the Mode III case, the elastic shear modulus G and the tangent modulus under simple shear G_{t} are used.

$$\partial(\ )/\partial t = (\dot{\ }) = -v\frac{\partial(\ )}{\partial x_1}. \tag{9}$$

By applying the principle of virtual work, and making use of the normalizations given in (8), and the steady-state condition (9) the (non-linear) finite element equilibrium equations can be derived [see Dean and Hutchinson (1980)].

A large rectangular domain which represents the upper half plane ($\hat{x}_2 \geqslant 0$) is modeled with rectangular finite elements which are placed parallel to the crack line ($\hat{x}_2 = 0$). The outer dimensions of the rectangular region are more than 10 times larger than the expected size of the crack-tip plastic zone. The mesh contains a total of 555 nodal points and 504 four-noded rectangular elements. The mesh near the crack tip is well refined with the size of the smallest element designed to be less than 1/600 of the maximum plastic zone extent. This is expected to accurately resolve the near-tip fields. Traction and/or displacement boundary conditions based on the elastic K-field are specified on the outer boundary of the mesh. Traction-free boundary condition is imposed on the crack flank ($\hat{x}_1 < 0, \hat{x}_2 = 0$) and u_3 displacement is constrained to be zero on the line ahead of the crack tip ($\hat{x}_1 \geqslant 0, \hat{x}_2 = 0$).

3.2. *Mode I plane stress crack growth*

In this case, the crack-tip coordinates (x_1, x_2), displacements u_i, stresses σ_{ij} and strains ε_{ij} are normalized as follows:

$$\left.\begin{aligned} \hat{x}_i &= x_i/(K/\sigma_0)^2 \\ \hat{u}_i &= u_i/(K^2/E\sigma_0) \\ \hat{\varepsilon}_{ij} = \varepsilon_{ij}/\varepsilon_0 \quad &\text{and} \quad \hat{\sigma}_{ij} = \sigma_{ij}/\sigma_0 \end{aligned}\right\}. \tag{10}$$

Here, σ_0 is the initial tensile yield stress, $\varepsilon_0 = \sigma_0/E$ is the initial tensile yield strain, E is the Young's modulus and K is the remote stress intensity factor. As mentioned earlier, the finite element equilibrium equations can be derived from the principle of virtual work and by making use of the steady-state condition (9) and the normalizations given in the above equation [see Dean and Hutchinson (1980)].

A large rectangular domain (with dimensions of more than 10 times the crack-tip plastic zone) representing the upper half plane ($\hat{x}_2 \geqslant 0$) is modeled with finite elements. A total of 429 nodal points and 384 four-noded rectangular elements has been used in this mesh. Traction and/or displacement boundary conditions based on the elastic K-field are specified along the outer boundary of the mesh. The smallest element length near the crack tip is designed to be less than 1/100 of the plastic zone size to provide good resolution.

An iterative procedure [see Dean and Hutchinson (1980)] is used to solve the non-linear finite element equilibrium equations. An important aspect in the numerical solution of elastic–plastic problems is the updating of plastic strains, internal variables and stresses. In the present analysis, these quantities at a certain point $(\hat{x}_1, \hat{x}_2)$ should be obtained by integrating eqns (4)–(7) from the elastic–plastic boundary in the negative $\hat{x}_1$ direction along a line holding $\hat{x}_2$ constant. An explicit integration procedure (with sub-incrementation) is used for this purpose.

4. RESULTS AND DISCUSSION

4.1. *Mode III crack growth*

The accuracy of the present computations is first assessed by comparing the near-tip stress distribution with the analytical asymptotic results of Castañeda (1987) for linear isotropic hardening. In his work, the near-tip stress variation is assumed to be of the type r^s, where r is the radial distance measured from the crack tip and s (which is a negative

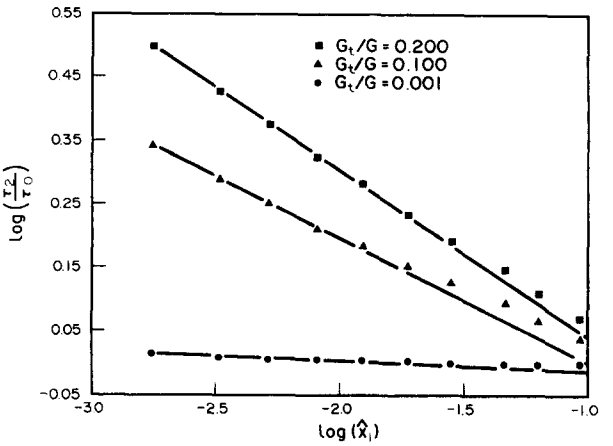

Fig. 1. Variation of $\log(\tau_2/\tau_0)$ with $\log(\hat{x}_1)$, where $\hat{x}_1$ is normalized distance ahead of the crack tip, corresponding to Mode III crack growth in isotropic hardening materials.

exponent) represents the order of the stress singularity. In Fig. 1, the variation of $\log(\tau_2/\tau_0)$ with $\log(\hat{x}_1)$, where $\hat{x}_1 = x_1/(K/\tau_0)^2$ is the normalized distance ahead of the crack tip, is presented for three different values of the hardening parameter G_t/G. The length scale over which the radial variations are plotted in this figure extends to about $x_1 = 0.1(K/\tau_0)^2$. This is well within the plastic zone size R_p which is between 0.2 and $0.3(K/\tau_0)^2$ ahead of the crack tip. Also shown in Fig. 1 are straight lines fitted (using the least-squares method) to the four points nearest to the crack tip.

It is clear from these plots that near the crack tip the stresses obtained from the finite element solution follow an r^s variation as assumed in the work of Castañeda (1987). It should be noted that as the level of hardening decreases, the stress singularity falls and for $G_t/G = 0.001$, which almost corresponds to the perfectly plastic case, τ_2 approaches a constant value of τ_0 except, perhaps, very close to the crack tip. The singularity order s obtained as the slope of the best-fit straight lines in Fig. 1 is found to be -0.261 and -0.196 for $G_t/G = 0.2$ and 0.1, respectively. These values agree well with Castañeda's results which are -0.277 and -0.207 corresponding to the above G_t/G ratios.

In Fig. 2, the near-tip angular variation of the normalized polar stress components τ_r/τ_0 and τ_θ/τ_0 obtained from the finite element solution is compared with the asymptotic results of Castañeda (1987). The centroidal values of stresses in the elements lying on a rectangular contour surrounding the moving crack tip, which is shown in the inset of Fig. 2, have been used to construct this plot. It must be noted that the distance of this contour

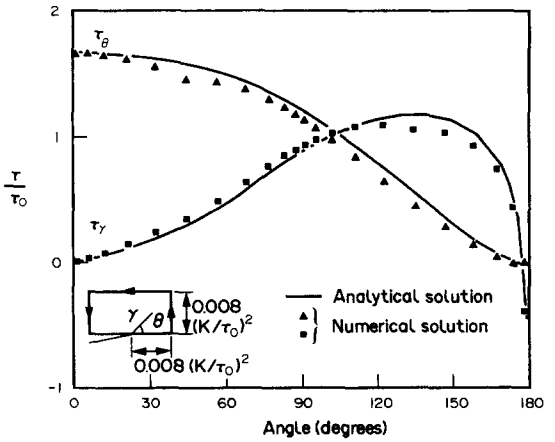

Fig. 2. Comparison of near-tip angular stress variation between analytical (Castañeda, 1987) and numerical solutions corresponding to Mode III crack growth in an isotropic hardening material with $G_t/G = 0.1$.

from the crack tip is 0.008 $(K/\tau_0)^2$ (which is within 3% of the plastic zone size R_p). In order to have a common basis for comparison, the normalized asymptotic stress variation reported by Castañeda (1987) has been scaled so that τ_2 stress at $\theta = 0$ matches with that obtained from the finite element solution. The results presented in Fig. 2 correspond to isotropic hardening with $G_t/G = 0.1$.

It can be seen from Fig. 2 that the agreement between the analytical and numerical results is quite close. It can be observed that both solutions show that τ_r is negative on the crack flank. No secondary plastic reloading along the crack flank has been detected for this case. However, the finite element results showed the existence of a tiny secondary reloading wake on the crack flank for smaller G_t/G ratios (less than 0.05). This corroborates the observations of Castañeda (1987) based on his asymptotic analysis. The good comparison with the analytical results as discussed above indicates that the present finite element simulation provides an accurate modelling of the near-tip fields. The influence of the Bauschinger effect on the stress and deformation fields near the crack tip and on the potential of the material for sustaining stable crack extension is investigated below.

The near-tip angular stress distribution obtained from the finite element solution (at a distance of 0.008 $(K/\tau_0)^2$ from the crack tip) is shown in Fig. 3 for both isotropic and kinematic hardening corresponding to $G_t/G = 0.2$. The difference in the stress distribution for the two hardening theories is not very significant, except, perhaps, in the variation of τ_r in the angular range $90° < \theta < 180°$. Also, it should be mentioned that while no secondary plastic reloading was detected on the crack flank for isotropic hardening (corresponding to $G_t/G = 0.2$), the results for kinematic hardening indicated secondary reloading as $\theta \to 180°$. These differences in the stress fields for kinematic hardening are clearly outcomes of the Bauschinger effect.

It is important to understand at this stage the stress history experienced by a material particle (which is just above the plane of crack propagation) as the crack tip passes underneath it. For this purpose, the stress history at a material point which successively occupies positions (relative to the moving crack tip) that correspond to the centroids of elements in the row adjacent to the crack plane is presented in Fig. 4. Results are given for both isotropic and kinematic hardening with $G_t/G = 0.1$. The points A, B, etc. on these curves correspond to locations relative to the current crack tip as indicated in the inset diagram of Fig. 4. Also shown in Fig. 4 is the locus of the center of the yield surface for the kinematic hardening case during the above loading history. Firstly, it should be noted that till the material point attains position A with respect to the propagating crack tip, the loading history experienced by it is almost proportional. Then as it occupies positions B, C and D relative to the crack tip it experiences strong non-proportional loading which is accompanied by a substantial change in the direction of the normal to the yield surface.

It is found that for the isotropic hardening case, plastic yielding continues to occur till point C. There is mild strain hardening as the stress state changes from A to C as evidenced

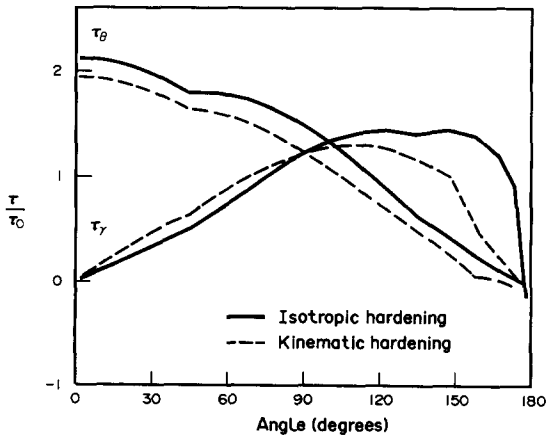

Fig. 3. Comparison of near-tip angular stress variation (at $r = 0.008(K/\tau_0)^2$) for Mode III crack growth between isotropic and kinematic hardening with $G_t/G = 0.2$.

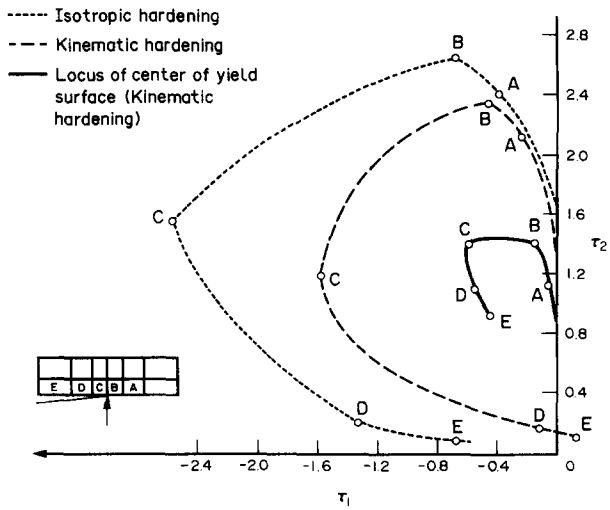

Fig. 4. Stress history experienced by a material element just above the crack plane during Mode III crack growth in isotropic and kinematic hardening materials with $G_t/G = 0.1$.

by the increase in radial distance from the origin of the τ_1, τ_2 axes. Elastic unloading begins at point C and no plastic reloading is observed as the material point recedes further behind the moving crack tip. By contrast, for the kinematic hardening case, all points A through E delineated in the stress history of Fig. 4 are yielded. This is clearly seen from the locus traced by the center of the yield surface as the stress state changes from A to E. The plastic yielding continues to occur beyond point E. On comparing the stress histories for the two hardening cases, it is found that they are about the same till the material point occupies position A relative to the crack tip. The difference between the two curves becomes significant as the tip passes underneath the material point (i.e. from B to E in Fig. 4). It must be noted that the material point under consideration is just above the crack plane. The stress history experienced by a point further removed from the crack plane is expected to be different and elastic unloading may occur even for the kinematic hardening case.

The normalized crack opening profile, $\delta/(J/\tau_0)$, is shown as a function of normalized distance $\hat{x}_1$ behind the crack tip in Figs 5 and 6. Here J represents the far-field J integral which is related to the remote stress intensity factor by $J = K^2/G$ for Mode III. The results presented in Figs 5 and 6 are for isotropic and kinematic hardening corresponding to $G_t/G = 0.2$ and 0.05, respectively. It can be seen from these figures that the crack opening

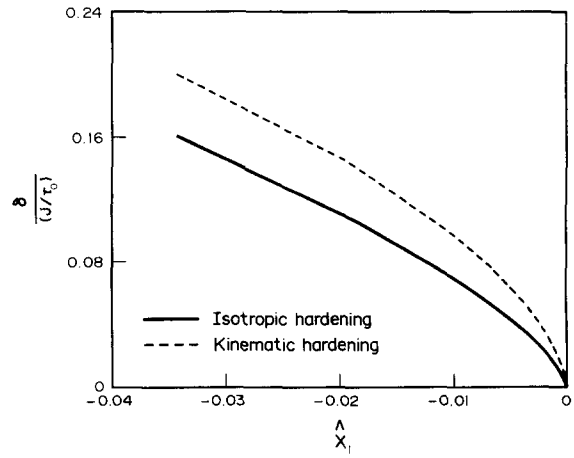

Fig. 5. Crack opening profiles for Mode III crack growth in isotropic and kinematic hardening materials with $G_t/G = 0.2$.

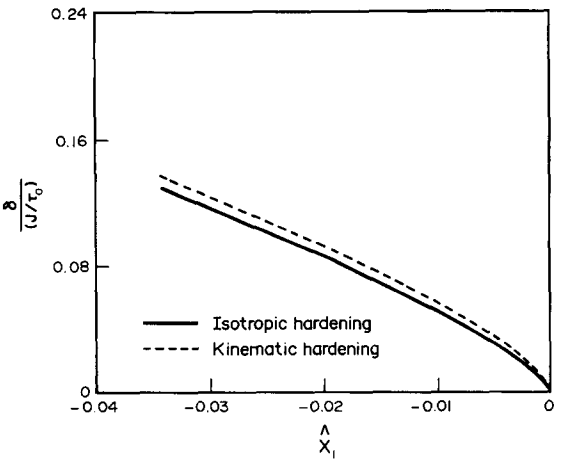

Fig. 6. Crack opening profiles for Mode III crack growth in isotropic and kinematic hardening materials with $G_t/G = 0.05$.

displacement at a given distance behind the crack tip is larger for kinematic hardening as compared to the isotropic hardening case.

In order to understand the above discrepancy, it is necessary to consider the stress histories given in Fig. 4. As seen from this figure, a material point just above the crack plane experiences predominantly proportional loading till the extending crack tip approaches it. During this phase, the normal to the yield surface in stress space does not change much and is almost coincident with the direction of the stress increment (which is radial). This results in considerable plastic strain accumulation at the material point. On the other hand, as the crack tip passes underneath it, strong non-proportional loading occurs (see Fig. 4). An elastic–plastic material offers more resistance to non-proportional loading histories than to proportional ones. This is attributed to the rotation of the normal to the yield surface and also to the fact that the direction of the stress increment is no longer coincident with the normal to the yield surface.

However, the resistance offered by an elastic–plastic material to non-proportional loading is diminished if it exhibits kinematic hardening (as opposed to isotropic hardening). Thus larger plastic strains would accumulate at the material point as the crack tip passes underneath it for the kinematic hardening case and this results in a larger crack opening profile. On comparing Figs 5 and 6, it is clear that the difference between the crack opening profiles for the two hardening cases becomes less as G_t/G decreases (i.e. as the perfectly plastic limit is approached).

As mentioned in the introduction, one of the main objectives of this work is to study the influence of the Bauschinger effect on the capacity of the material to sustain slow, stable crack growth. For this purpose, the ratio of the far-field J integral for steady-state crack growth to its value at initiation (J_{ss}/J_c), has been estimated using a critical crack tip opening displacement criterion. This criterion, proposed by Rice and Sorensen (1978), requires that a critical opening displacement, $\delta = \delta_c$ should be maintained at a small micro-structural distance, $r = r_c$, behind the crack tip for continued crack propagation. By employing this criterion to model both crack initiation and continued crack growth, the ratio J_{ss}/J_c was estimated as described below.

The crack opening profiles for steady-state crack growth shown in Figs 5 and 6 were used to obtain the variation of $\delta/(\gamma_0 r)$ with normalized distance $r/(K/\tau_0)^2$, measured from the crack tip along the crack flank. For a given value of the critical micro-scale parameter, $\delta_c/(\gamma_0 r_c)$, the value of $r_c/(K_{ss}/\tau_0)^2$ was obtained from this variation corresponding to steady-state crack growth. In order to model crack initiation, the results given by Rice (1967) for the stationary crack problem pertaining to Mode III small-scale yielding conditions is employed. It can be shown from Rice (1967) [see also Dean and Hutchinson (1980)] that the relation between the crack opening displacement δ and the distance r behind the crack tip for linear strain hardening is given by:

$$\hat{r} = \begin{cases} -\left(\dfrac{\alpha}{1-\alpha}\right)\left[\dfrac{\hat{\delta}}{2} + \dfrac{1}{\pi(1-\alpha)} \ln\left(1 - \dfrac{\pi}{2}(1-\alpha)\hat{\delta}\right)\right], & \hat{\delta} < \dfrac{2}{\pi}, \\ \dfrac{\pi}{8}\hat{\delta}^2 - \dfrac{\alpha}{\pi(1-\alpha)^2}(1-\alpha+\ln\alpha) - \dfrac{1}{2\pi}, & \hat{\delta} \geqslant \dfrac{2}{\pi}. \end{cases}$$

In this equation, $\hat{r} = r/(K/\tau_0)^2$ and $\hat{\delta} = \delta/(J/\tau_0)$ are normalized quantities and $\alpha = G_t/G$. From this relation, the value of $r_c/(K_c/\tau_0)^2$ corresponding to a certain value of $\delta_c/(\gamma_0 r_c)$ was obtained. The two quantities, $r_c/(K_{ss}/\tau_0)^2$ and $r_c/(K_c/\tau_0)^2$ were then used to compute the ratio $J_{ss}/J_c = (K_{ss}/K_c)^2$ corresponding to the chosen value of the micro-structural parameter $\delta_c/(\gamma_0 r_c)$.

The variation of J_{ss}/J_c with $\delta_c/(\gamma_0 r_c)$, calculated as indicated above, is shown in Fig. 7 for isotropic and kinematic hardening corresponding to $G_t/G = 0.05$ and 0.1. From this figure, it can be seen that for a certain value of $\delta_c/(\gamma_0 r_c)$ (greater than about 2), the ratio J_{ss}/J_c for the kinematic hardening material is less than the isotropic hardening case. The difference between the two hardening cases increases with increase in the critical microscale parameter $\delta_c/(\gamma_0 r_c)$. It can further be observed from Fig. 7 that J_{ss}/J_c decreases with an increase in strain hardening (larger G_t/G). Also, as expected, the difference in J_{ss}/J_c between isotropic and kinematic hardening becomes more enhanced for larger G_t/G. Thus, for example, pertaining to $\delta_c/(\gamma_0 r_c) = 5$, it is found from Fig. 7 that J_{ss}/J_c is equal to 10 and 6 for isotropic and kinematic hardening, respectively, with $G_t/G = 0.1$. The corresponding values of J_{ss}/J_c for $G_t/G = 0.05$ are 16.5 and 11.5.

4.2. *Mode I plane stress crack growth*

As in the case of Mode III crack growth (Section 4.1), the near-tip angular stress distribution for linear isotropic hardening ($E_t/E = 0.1$), obtained from the numerical solution is first compared in Fig. 8 with the analytical asymptotic results given by Castañeda (1987). The numerical results plotted in Fig. 8 are taken along the rectangular contour indicated in the inset of the figure. It should be noted that this contour is taken at a distance of $0.014(K/\sigma_0)^2$ from the moving crack tip (which is within 5% of the plastic zone size). The normalized stress variation given by Castañeda has been appropriately scaled to enable comparison with the finite element results. It can be seen from Fig. 8 that the agreement between the analytical and numerical results is quite close. The angular variations in Fig. 8 are also similar in structure to the perfectly plastic results given by Narasimhan *et al.* (1987a). Castañeda (1987) has reported that the elastic unloading boundary makes an angle of $\theta = 73.6°$ with respect to the x_1 axis for $E_t/E = 0.1$. The present numerical results indicate that elastic unloading begins at around $\theta = 85°$.

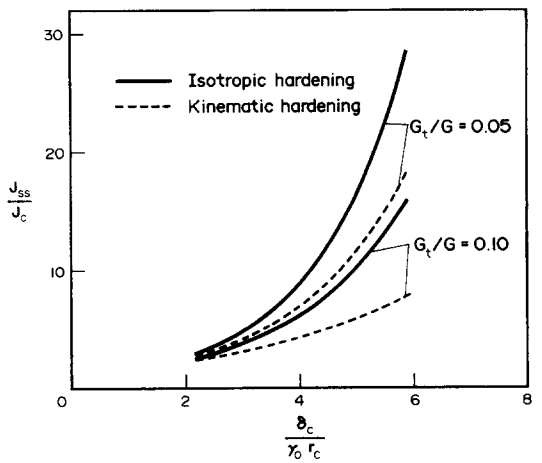

Fig. 7. Variation of J_{ss}/J_c with micro-structural parameter $\delta_c/(\gamma_0 r_c)$ for isotropic and kinematic hardening materials corresponding to Mode III.

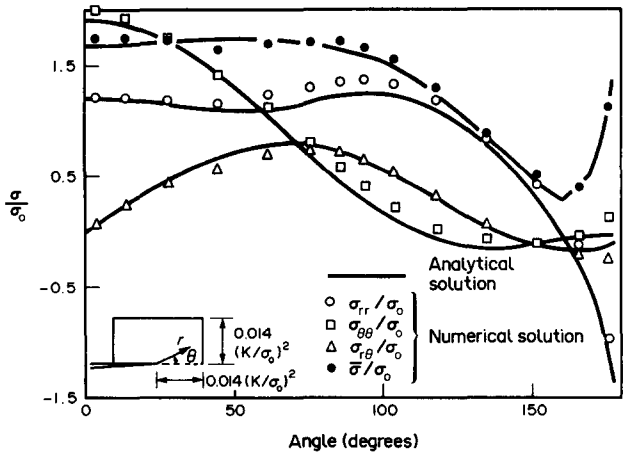

Fig. 8. Comparison of near-tip angular stress variation between analytical (Castañeda, 1987) and numerical solutions corresponding to Mode I plane stress crack growth in an isotropic hardening material with $E_t/E = 0.1$.

It can be observed from Fig. 8 that σ_{rr} obtained from the analytical and numerical solutions is negative on the crack flank ($\theta = 180°$). The analysis of Castañeda (1987) indicates that in the limit as $E_t/E \to 0$, secondary plastic reloading (in compression) will occur in a tiny angular sector adjacent to the crack flank. However, unlike in Mode III, secondary plastic reloading was not detected by the present numerical analysis for isotropic hardening for any value of E_t/E. Nevertheless, it can be seen from Fig. 8 that the von Mises equivalent stress, $\bar{\sigma} = \sqrt{3/2 S_{ij} S_{ij}}$, obtained from the numerical solution increases strongly as $\theta \to 180°$ which conforms to the analytical result. In order to fully resolve the issue pertaining to plastic reloading, very thin elements may have to be placed adjacent to the crack flank.

In Fig. 9, the near-tip angular stress distribution [at a distance of $0.014(K/\sigma_0)^2$ from the tip] is displayed for isotropic and kinematic hardening corresponding to $E_t/E = 0.2$. It can be observed that the stresses based on the kinematic hardening theory are, in general, lower than those for isotropic hardening. However, the decrease in the stresses all around the crack tip for the kinematic hardening material as observed in Fig. 9 is not as dramatic as in the Mode I plane strain case [see Lam and McMeeking (1984)]. The decrease in stress triaxiality ahead of the propagating tip for Mode I plane strain, as observed in the work of Lam and McMeeking (1984), is expected to affect the growth of micro-voids, whereas no such implications arise for the plane stress case.

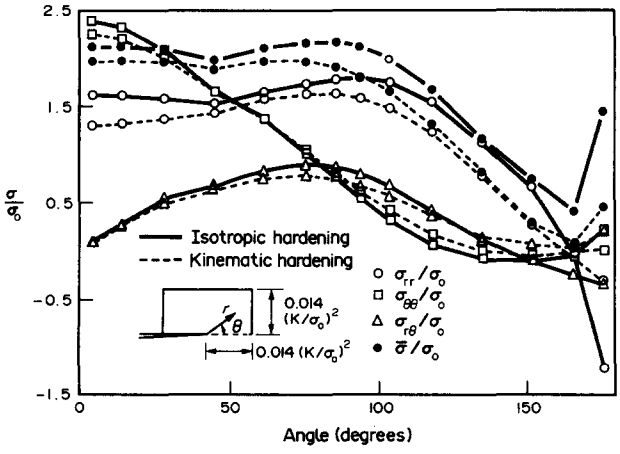

Fig. 9. Comparison of near-tip angular stress variation for Mode I plane stress crack growth between isotropic and kinematic hardening with $E_t/E = 0.2$.

From Fig. 9, it can be seen that the maximum difference between isotropic and kinematic hardening occurs in the angular distribution of σ_{rr}. This is particularly evident behind the crack tip ($\theta > 90°$). For isotropic hardening, there is a significant state of compression on the crack flank as indicated by the large negative value of σ_{rr} as $\theta \to 180°$. Also, as noted above, there is a tendency for the von Mises equivalent stress $\bar{\sigma}$ to increase adjacent to $\theta = 180°$. On the other hand, for kinematic hardening, the negative value of σ_{rr} and the magnitude of $\bar{\sigma}$ on the crack flank are considerably less. However, due to the translation of the yield surface, secondary plastic reloading has taken place on the crack flank for kinematic hardening. The above noted features in the stress distribution for kinematic hardening are caused by the Bauschinger effect in the reversed plastic flow region along the crack flank.

The active plastic zones surrounding the steadily propagating crack tip are shown in normalized crack-tip coordinates $(\hat{x}_1, \hat{x}_2)$ in Fig. 10 for isotropic and kinematic hardening with $E_t/E = 0.2$. The elements inside the active plastic zone are currently experiencing plastic deformation. The elements behind the trailing boundary of the active plastic zone constitute the elastic unloading wake. These elements have residual plastic strains but are currently deforming in an (incremental) elastic manner.

The plastic zone for isotropic hardening is similar in shape and size to that reported by Dean (1983). On comparing the plastic zones for the two hardening cases, it can be seen that the extent of plastic yielding ahead of the crack tip is slightly more for kinematic hardening. However, the maximum difference between the two plastic zones occurs behind the crack tip. It can be seen that the trailing boundary of the active plastic zone spreads further behind the crack tip for kinematic hardening. Also, a secondary plastic reloading region adjacent to the crack flank can be observed for this case. This is not present for isotropic hardening. As noted earlier, in connection with the near-tip angular stress distribution, reversed plastic yielding on the crack flank occurs for kinematic hardening due to the translation of the yield surface. This can be understood further by referring to the stress histories presented in Fig. 4 for the Mode III case which has qualitatively similar features as Mode I plane stress.

The variation of the normalized crack opening displacement, $\delta/(J/\sigma_0)$, with normalized distance $\hat{x}_1$ along the crack flank is shown in Fig. 11 for isotropic and kinematic hardening corresponding to $E_t/E = 0.2$. Here, J denotes the value of the far-field J integral, which is related to the remote stress intensity factor K by $J = K^2/E$ for Mode I plane stress. It can be seen that the crack opening displacement at a given distance behind the crack tip is higher for kinematic hardening as compared to isotropic hardening. As explained in Section 4.1, this difference is an outcome of the lowered resistance offered by a kinematic hardening material to non-proportional loading that occurs in the vicinity of the propagating crack tip.

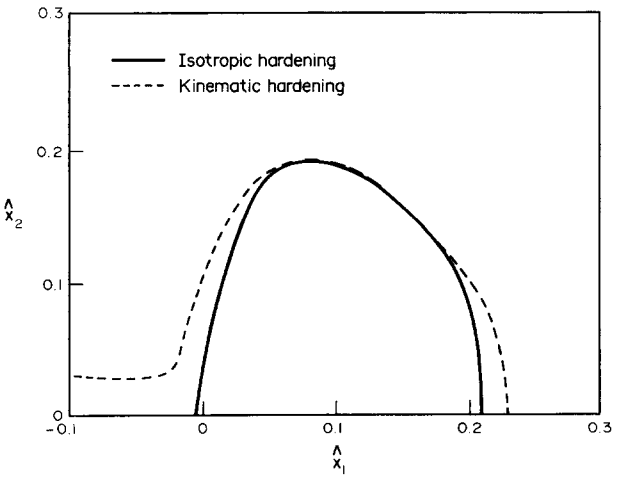

Fig. 10. Active plastic zones surrounding the propagating crack tip (under Mode I plane stress) for isotropic and kinematic hardening materials with $E_t/E = 0.2$.

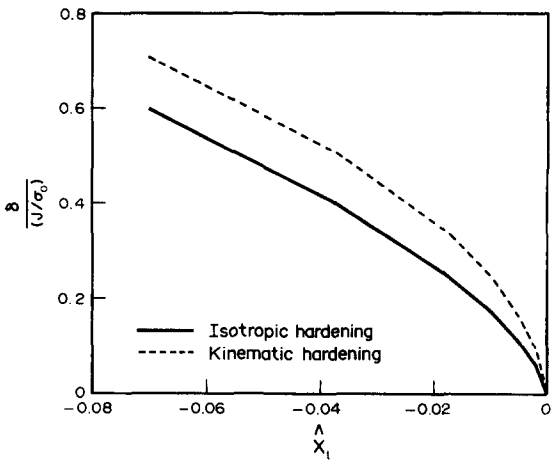

Fig. 11. Crack opening profiles for Mode I plane stress crack growth in isotropic and kinematic hardening materials with $E_t/E = 0.2$.

The critical crack opening displacement criterion is imposed simultaneously on the steady-state crack opening profiles (like the one shown in Fig. 11) and stationary crack opening profiles to obtain the ratio J_{ss}/J_c (see Section 4.1 for details). However, unlike in Mode III, no full-field analytical solution is available for the stationary crack problem under Mode I plane stress. Hence, a separate finite element analysis of the monotonic loading of a stationary crack in a linear hardening material was performed [analogous to Narasimhan and Rosakis (1988)]. The stationary crack opening profiles required to estimate J_{ss}/J_c were obtained from this analysis.

The variation of J_{ss}/J_c with the micro-structural parameter $\delta_c/(\varepsilon_0 r_c)$ is shown in Figs 12(a) and (b) for $G_t/G = 0.2$ and 0.05, respectively. Results are presented for both isotropic and kinematic hardening. These figures clearly demonstrate that for a given value of $\delta_c/(\varepsilon_0 r_c)$ (greater than about 7 or so), the ratio J_{ss}/J_c for the kinematic hardening case is significantly less than isotropic hardening. The variations shown in Figs 12(a) and (b) are qualitatively similar to Mode III (see Fig. 7).

5. CONCLUSIONS

In this paper, steady-state crack growth under Mode III and Mode I plane stress in materials displaying linear isotropic and kinematic hardening has been analysed. The following are the important conclusions of this work:

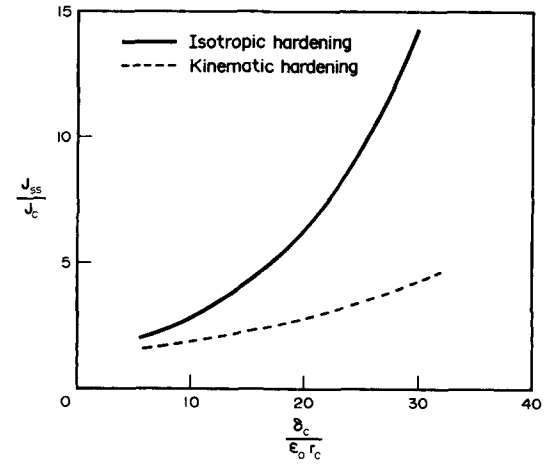

Fig. 12(a). Variation of J_{ss}/J_c with micro-structural parameter $\delta_c/(\varepsilon_0 r_c)$ for isotropic and kinematic hardening materials ($E_t/E = 0.2$) corresponding to Mode I plane stress.

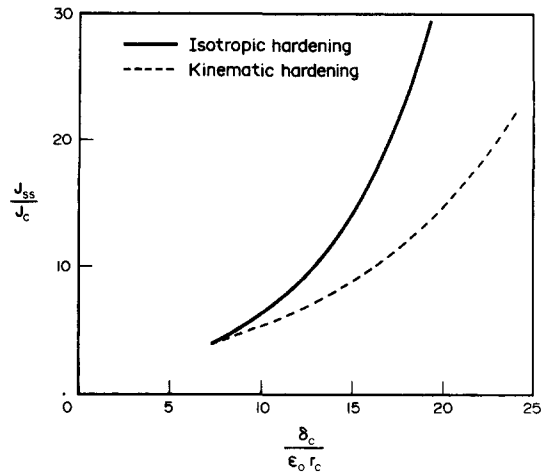

Fig. 12(b). Variation of J_{ss}/J_c with micro-structural parameter $\delta_c/(\varepsilon_0 r_c)$ for isotropic and kinematic hardening materials ($E_t/E = 0.05$) corresponding to Mode I plane stress.

(1) The near-tip angular stress distribution for kinematic hardening does not deviate significantly from isotropic hardening for Mode III and Mode I plane stress. The maximum difference in the stresses for the two hardening cases occurs behind the crack tip (i.e. $\theta > 90°$).
(2) The results for kinematic hardening corresponding to both Mode III and Mode I plane stress indicate the presence of a substantial secondary plastic reloading region along the crack flank. For isotropic strain hardening, a tiny secondary reloading region was detected by the numerical solution for Mode III in the perfectly plastic limit (i.e. for very small G_t/G ratios), which is in conformity with the asymptotic analysis of Castañeda (1987). However, no such region was observed for isotropic strain hardening in the case of Mode I plane stress.
(3) An examination of the stress history experienced by a material point immediately above the crack plane for Mode III reveals that it is almost proportional till the crack tip approaches it and is quite the same for isotropic and kinematic hardening. However, as the crack tip passes underneath the point strong non-proportional loading occurs and the stress histories for the two hardening cases show significant differences. Of particular importance is the fact that elastic unloading occurs in the case of isotropic hardening as the crack tip leaves the material point behind it, whereas continued yielding occurs for kinematic hardening.
(4) The (normalized) crack opening displacement at a certain (normalized) distance behind the tip is larger for kinematic hardening as compared to isotropic hardening. This is attributed to the reduced resistance offered by a kinematic hardening material to non-proportional loading that is experienced near the propagating crack tip.
(5) The results demonstrate that the potential of an elastic–plastic material for sustaining slow, stable crack growth under Mode III or Mode I plane stress, as reflected by the ratio J_{ss}/J_c, will be drastically diminished if it exhibits the Bauschinger effect. Analogous conclusions for Mode I plane strain have been made by Lam and McMeeking (1984).

In Part II of this work, a direct finite element simulation of crack initiation and stable crack growth is undertaken within the context of Mode I plane stress, small-scale yielding conditions. This is achieved by imposing the critical crack opening displacement criterion described in Section 4.1 of this paper. The analysis predicts the resistance curve for stable crack growth. The main objectives of the investigation are to examine the influence of the Bauschinger effect on the tearing resistance of the material and the extent to which it can accommodate stable crack extension.

Acknowledgement—The second author wishes to gratefully acknowledge the Aeronautics Research and Development Board (Government of India) for financial support through sponsored project No. Aero/RD-134/100/519.

REFERENCES

Amazigo, J. C. and Hutchinson, J. W. (1977). Crack tip fields in steady crack growth with linear strain hardening. *J. Mech. Phys. Solids* **25,** 81–97.

Castañeda, P. P. (1987). Asymptotic fields in steady crack growth with linear strain hardening. *J. Mech. Phys. Solids* **35,** 227–268.

Chitaley, A. D. and McClintock, F. A. (1971). Elastic–plastic mechanics of steady crack growth under anti-plane shear. *J. Mech. Phys. Solids* **19,** 147–163.

Dean, R. H. (1983). Elastic–plastic steady crack growth in plane stress. In *Elastic–Plastic Fracture: Second Symposium. Vol I:* Inelastic Crack Analysis, *ASTM STP 803* (Edited by C. F. Shih and J. F. Gudas), pp. 39–51. ASTM, Philadelphia, PA.

Dean, R. H. and Hutchinson, J. W. (1980). Quasi-static crack growth in small-scale yielding. In *Fracture Mechanics: Twelfth Conference, ASTM STP 700*, pp. 383–405. ASTM, Philadelphia, PA.

Drugan, W. J., Rice, J. R. and Sham, T. L. (1982). Asymptotic analysis of growing plane strain tensile cracks in elastic-ideally plastic solids. *J. Mech. Phys. Solids* **30,** 447–473.

Lam, P. S. and McMeeking, R. M. (1984). Analysis of steady, quasi-static crack growth in plane strain tension in elastic–plastic materials with non-isotropic hardening. *J. Mech. Phys. Solids* **32,** 395–414.

Narasimhan, R. and Rosakis, A. J. (1988). A finite element analysis of small-scale yielding near a stationary crack under plane stress. *J. Mech. Phys. Solids* **36,** 77–117.

Narasimhan, R., Rosakis, A. J. and Hall, J. F. (1987a). A finite element study of stable crack growth under plane stress conditions: Part I—Elastic–perfectly plastic solids. *Trans. ASME J. Appl. Mech.* **54,** 838–845.

Narasimhan, R., Rosakis, A. J. and Hall, J. F. (1987b). A finite element study of stable crack growth under plane stress conditions: Part II—Influence of hardening. *Trans. ASME J. Appl. Mech.* **54,** 846–853.

Rice, J. R. (1967). Stresses due to a sharp notch in a work hardening elastic–plastic material loaded by longitudinal shear. *Trans. ASME J. Appl. Mech.* **34,** 287–298.

Rice, J. R. (1975). Elastic–plastic models for stable crack growth. In *Mechanics and Mechanisms of Crack Growth* (Edited by M. J. May), pp. 14–39. British Steel Corp. Physical Metallurgy Centre Publications, Sheffield.

Rice, J. R. and Sorensen, E. P. (1978). Continuing crack tip deformation and fracture for plane strain crack growth in elastic–plastic solids. *J. Mech. Phys. Solids* **26,** 163–186.

Sham, T. L. (1983). A finite element study of asymptotic near-tip fields for Mode I plane strain cracks growing stably in elastic-ideally plastic solids. In *Elastic–Plastic Fracture: Second Symposium: Vol I—Inelastic Crack Analysis, ASTM STP 803* (Edited by C. F. Shih and J. F. Gudas), pp. 52–79. ASTM, Philadelphia, PA.

Zhang, R., Zhang, X. and Hwang, K. C. (1983). Near-tip fields for plane strain, mode I steady state crack growth in linear hardening materials with Bauschinger effect. In *Proceedings of ICF International Symposium on Fracture Mechanics*, pp. 283–290. Science Press, Beijing.